Self-Assembly at the Air−Water Interface. In-Situ Preparation of Thin Films of Metal Ion Grid Architectures

Isabelle Weissbuch,*,† Paul N. W. Baxter,⊥ Sidney Cohen,† Hagai Cohen,† Kristian Kjaer,‡ Paul B. Howes,‡ Jens Als-Nielsen,§ Gary S. Hanan,⊥ Ulrich S. Schubert,⊥ Jean-Marie Lehn,*,⊥ Leslie Leiserowitz,*,† and Meir Lahav*,†

Contribution from the Department of Materials & Interfaces, The Weizmann Institute of Science, 76100 Rehovot, Israel, Department of Solid State Physics, Risø National Laboratory, DK 4000, Roskilde, Denmark, Niels Bohr Institute, H. C. Ørsted Laboratory, DK 2100, Copenhagen, Denmark, and Laboratoire de Chimie Supramoléculaire Institut Le Bel, Université Louis Pasteur, F-67000 Strasbourg, France

Received January 20, 1998

Abstract: Oriented crystalline films, ∼11−20 Å thick, of metal ion complexes of the grid type $[Co_4L_4]^{8+}\cdot 8PF_6^-$ and $[Ag_9L_6]^{9+}\cdot 9CF_3SO_3^-$, based on various ligands *L*, were prepared in-situ at the air-aqueous solution interface by the interaction of the free ligand molecules spread onto aqueous solutions containing Co^{2+} or Ag^+ ions. The structure of the complex architectures composed of a 2×2 Co^{2+} grid coordinated to four ligand molecules and a 3×3 Ag^+ grid coordinated to six ligand molecules as well as their molecular organization in thin films were characterized by grazing incidence synchrotron X-ray diffraction (GIXD) and specular X-ray reflectivity (XR) measurements performed at the air-aqueous solution interface and by UV, X-ray photoelectron spectroscopy (XPS), and scanning force microscopy (SFM) after film transfer onto various solid supports. The results open perspectives toward an implementation of the air−water interface for the self-assembly and subsequent deposition of organized arrays of complex inorganic architectures onto solid support.

1. Introduction

The formation, at the air-aqueous solution interface, of crystallites, one to several layers thick, of water-insoluble molecules such as long-chain amides, diols, α-amino acids, alkanes, and oligothiophenes, has recently been reported.[1−5] More complex architectures have been generated by the interaction between the insoluble component and various solutes from the subphase. Examples include multilayers of divalent metal salts of dicarboxylic acids, ionophores, and interdigitated trilayers composed of long-chain acids and soluble amines.[6−8] We address whether this approach can be extended to supramolecular multicomponent systems.

The self-assembly of inorganic supramolecular systems in the form of racks, ladders, grids, and cages has recently been reported.[9−14] The coordination array in such systems may be assembled from either tridentate ligands and octahedral metal ions or from bidentate ligands and tetrahedral metal ions. A tetranuclear 2×2 cobalt^{2+} grid complex, $[Co_4L_4]^{8+}\cdot 8SbF_6^-$, of the ligand L = 4,6-bis(6-2,2′-bipyridyl))2-methylpyrimidine ***1*** and its derivatives (Scheme 1a), containing four ligands arranged two above and two below the plane of the four Co^{2+} ions, is an example of octahedral coordinated metal ions.[14] As an example of the second type of coordination, the complex between nine Ag^+ ions and six ligands, $[Ag_9L_6]^{9+}\cdot 9CF_3SO_3^-$ (Scheme 1b), forms a layered three-dimensional crystal structure when grown from a nitromethane solution.[12] The complex cations appear in the form of a 3×3 grid of the nine Ag^+ ions in a distorted tetrahedral environment with two chelating agents at each Ag^+ site. The six ligands, L = 6,6′-bis[2-(6-**R**-pyridyl)]-3,3′-bipyridazine **R** = methyl ***2*** (Scheme 1b), are divided into two sets of three, one above and one below the plane of the nine silver ions.

We envisaged that spreading the free ligand *L* molecules onto the surface of an aqueous solution containing metal ions could lead to the formation of the grid complex at the air−water interface. Once formed, the complex cations with counterions

† The Weizmann Institute of Science.
‡ Risø National Laboratory.
§ Niels Bohr Institute.
⊥ Université Louis Pasteur.

(1) Weinbach, S. P.; Bouwman, W. G.; Kjaer, K.; Als-Nielsen, J.; Lahav, M.; Leiserowitz, L. *J. Phys. Chem.* **1996**, *100*, 8356−8362.
(2) Popovitz-Biro, R.; Edgar, R.; Majewski, J.; Cohen, S.; Margulis, L.; Kjaer, K.; Als-Nielsen, J.; Leiserowitz, L.; Lahav, M. *Croat. Chem. Acta* **1996**, *69*, 689.
(3) Weinbach, S. P.; Weissbuch, I.; Kjaer, K.; Bouwman, W. G.; Als-Nielsen, J.; Lahav, M.; Leiserowitz, L. *Adv. Mater.* **1995**, *7*, 857.
(4) Isz, S.; Weissbuch, I.; Palacin, S.; Ruaudell-Texier, A.; Bouwman, W. G.; Kjaer, K.; Als-Nielsen, J.; Leiserowitz, L.; Lahav, M. *Chemistry A Eur. J.* **1997**, *3*, 930.
(5) Weissbuch, I.; Berfeld, M.; Bouwman, W. G.; Kjaer, K.; Als-Nielsen, Lahav, M.; Leiserowitz, L. *J. Am. Chem. Soc.* **1997**, *119*, 933.
(6) Weissbuch, I.; Guo, S.; Cohen, S.; Edgar, R.; Howes, P.; Kjaer, K.; Als-Nielsen, J.; Lahav, M.; Leiserowitz, L. *Adv. Mater.* **1998**, 117.
(7) Rappaport, H.; Kuzmenko, I.; Bouwman, W.; Kjaer, K.; Als-Nielsen, J.; Leiserowitz, L.; Lahav, M. *J. Am. Chem. Soc.* **1997**, *119*, 11211.
(8) Kuzmenko, I.; Buller, R.; Bouwman, W. G.; Kjaer, K.; Als-Nielsen, J.; Lahav, M.; Leiserowitz, L. *Science* **1996**, *274*, 2046−2049.
(9) Lehn, J.-M. *Supramolecular Chemistry Concepts and Perspectives*; VCH: Weinheim, Germany, 1995; Chapter 9, pp 139−197.
(10) Youinou, M.-T.; Rahmouni, N.; Fischer, J.; Osborn, J. A. *Angew. Chem., Int. Ed. Engl.* **1992**, *31*, 733.
(11) Baxter, P. N. W.; Lehn, J.-M.; DeCian, A.; Fischer, J. *Angew. Chem., Int. Ed. Engl.* **1993**, *32*, 69.
(12) Baxter, P. N. W.; Lehn, J.-M.; Fischer, J.; Youinou, M.-T. *Angew. Chem., Int. Ed. Engl.* **1994**, *33*, 2284.
(13) Hanan, G. S.; Arana, C. R.; Lehn, J.-M.; Fenske, D. *Angew. Chem., Int. Ed. Engl.* **1995**, *34*, 1122.
(14) Hanan, G. S.; Volmer, D.; Schubert, U. S.; Lehn, J.-M.; Baum, G.; Fenske D. *Angew. Chem., Inter. Ed. Engl.* **1997**, *36*, 1842.

S0002-7863(98)00205-4 CCC: $15.00
Published on Web 05/02/1998

Scheme 1

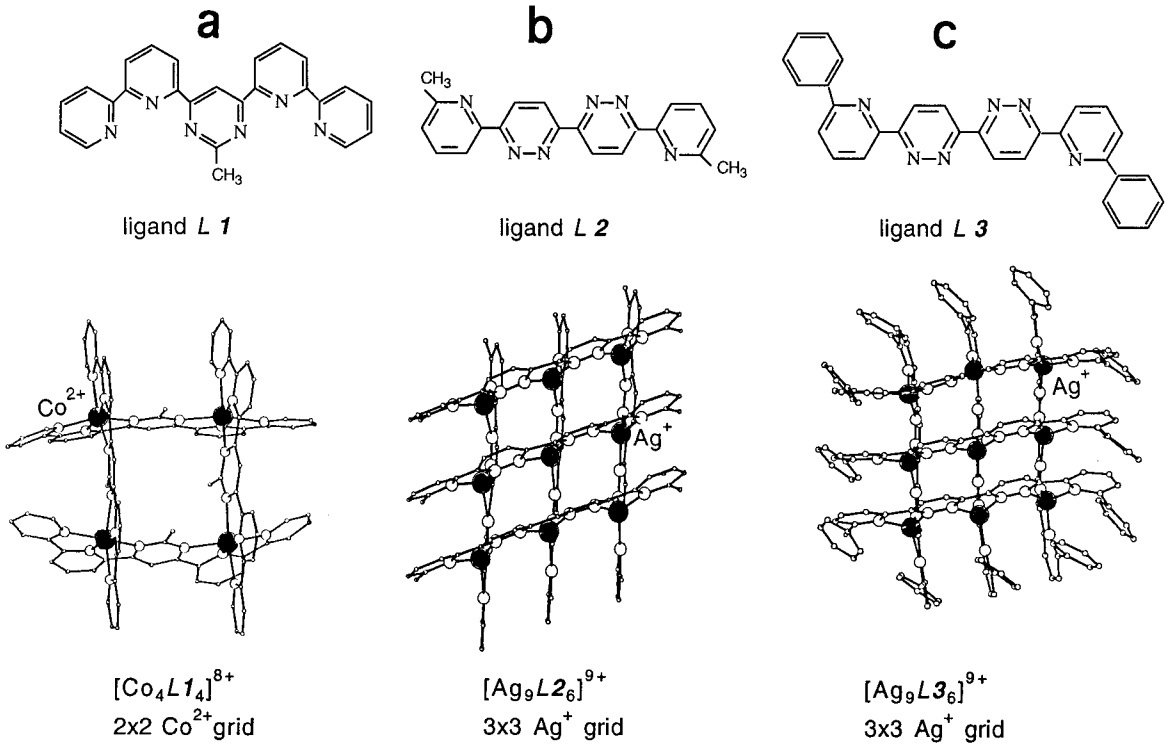

(that make the salt insoluble in water) would form amorphous films at the solution surface or self-assemble into crystalline domains of structure akin to that of the macroscopic crystal. A lateral aggregation process being favored at interfaces, the resulting structure must contain a small number of layers. Such films prepared by self-assembly and transferred to solid surfaces may be of interest for microelectronic technology.

Here we report on the self-assembly of various metal ion grid complexes as two-dimensional films at the air-aqueous solution interface in order to demonstrate the potential of this approach. The 2×2 Co^{2+} grid complex of ligand ***1*** (Scheme 1a) forms poorly ordered films; on the other hand, the 3×3 Ag^+ grids starting from the two free ligands ***2*** and ***3*** (Scheme 1b,c) form highly crystalline domains with a specific orientation at the air-aqueous solution interface. The crystalline structures, at the air−solution interface, were examined by grazing incidence X-ray diffraction (GIXD) and specular X-ray reflectivity (XR) using synchrotron radiation. The films were transferred from the interface onto various solid supports and characterized by UV spectroscopy, X-ray photoelectron spectroscopy (XPS), and scanning force microscopy (SFM). In view of the complexity of the process, involving first reaction followed by crystalline self-assembly of the multicomponent systems, a variety of methods are necessary to characterize the film structure, each method revealing a different aspect, be it molecular structure or supramolecular organization.

2. Experimental Section

Materials. The ligands *L*, 4,6-bis(6-2,2′-bipyridyl))2-methylpyrimidine ***1***, 6,6′-bis[2-(6-methylpyridyl)]-3,3′-bipyridazine ***2***, and 6,6′-bis[2-(6-phenylpyridyl)]-3,3′-bipyridazine ***3*** (synthesis described elsewhere[12,15]), were spread from 0.5 mM solutions in chloroform. The 2×2 Co^{2+} complex of ligand ***1***, $[Co_4L_4]\cdot 8PF_6$, and 3×3 Ag^+ complexes of ligands ***2*** and ***3***, $[Ag_9L_9]\cdot 9CF_3SO_3$, were prepared in bulk solution as described elsewhere.[12,14] Commercially available silver triflate, cobalt acetate, and ammonium hexafluorophosphate have been used.

The surface pressure−area (Π-A) isotherms were performed on a automatic Lauda trough, in dark when silver triflate aqueous solutions were used.

Grazing Incidence X-ray Diffraction (GIXD). The experiments were performed on the liquid surface diffractometer[16] at the undulator BW1 synchrotron beam line Hasylab, DESY (Hamburg). When silver triflate solutions were used as subphase, the film preparation was done in red light. Measurements were performed, at different points along the isotherms and at 5 °C. A detailed description of the GIXD method is given elsewhere.[17] The scattered intensity was detected by a position-sensitive detector (PSD) along the vertical component of the X-ray scattering vector $q_z \approx (2\pi/\lambda)\sin \alpha_f$, α_f being the angle between the horizon and the diffracted beam. Measurements were performed by scanning over a range along the horizontal scattering vector $q_{xy} \approx (4\pi/\lambda)\sin \theta_{xy}$, where $2\theta_{xy}$ is the angle between the incident and diffracted beams projected onto the horizontal plane. The diffraction data are represented in two ways: the GIXD pattern $I(q_{xy})$ obtained by integrating over the whole q_z window of the PSD shows Bragg peaks; Bragg rod intensity profiles are the scattered intensity $I(q_z)$ recorded in channels along the PSD but integrated across the q_{xy} range of each Bragg peak. The GIXD pattern can be also presented as a two-dimensional intensity distribution $I(q_{xy},q_z)$.

Several different types of information were extracted from the measured profiles. The $2\theta_{xy}$ (or q_{xy}) positions of the Bragg peaks yield the lattice repeat distances $d = 2\pi/q_{xy}$ which can be indexed by two indices h,k to yield the unit cell. The full width at half-maximum of the Bragg peaks along q_{xy}, fwhm(q_{xy}), yields an estimate of the 2D crystalline coherence length, $L \approx 0.88 \cdot 2\pi/\text{fwhm}(q_{xy})$. The fwhm of the Bragg rod intensity profile along q_z, fwhm(q_z), gives an estimate of the crystallite thickness $\approx 0.88 \cdot 2\pi/\text{fwhm}(q_z)$. The separation along q_z between various intensity modulations gives an estimate of the lattice spacing in the direction perpendicular to the liquid surface $\approx 2\pi/\Delta q_z$. The intensity at a particular value in a Bragg rod is determined by the

(15) Hanan, G. S.; Schubert, U. S.; Volkmer, D.; Rivière, E.; Lehn, J.-M.; Kyritsakas, N.; Fischer, J. *Can. J. Chem.* **1997**, *75*, 169.

(16) Majewski, J.; Popovitz-Biro, R.; Bouwman, W. G.; Kjaer, K.; Als-Nielsen, J.; Lahav, M.; Leiserowitz, L. *Chem. Eur. J.* **1995**, *1*, 304.

(17) Als-Nielsen, J.; Jacquemain, D.; Kjaer, K.; Leveiller, F.; Lahav, M.; Leiserowitz, L. *Physics Reports* **1994**, *246(5)*, 251.

square of the molecular structure factor $|F_{hk}(q_z)|^2$ thus allowing its evaluation according to an atomic coordinate model of the molecules.[18]

Specular X-ray Reflectivity (XR). Measurements, using the same liquid surface diffractometer as for the GIXD, were performed by scanning the incident (α_i), equal to the reflected (α_r) beam angles from $0.5\alpha_c$ to $35\alpha_c$, where $\alpha_c = 0.138°$ is the critical angle for total external reflection.[17] The detection of the reflected radiation was measured by a NaI scintillation counter. The experimental results are given in the form of normalized X-ray reflectivity R/R_F, where R_F is the "Fresnel" reflectivity calculated for a perfect sharp interface, as a function of the normalized vertical scattering vector q_z/q_c, where $q_z = (4\pi/\lambda)\sin\alpha_r$ and q_c is the scattering vector at the critical angle of incidence.

UV, XPS, and SFM. Measurements were performed on samples prepared in a specially constructed Teflon trough (surface area 20 cm^2) in which the solid supports were inserted into the subphase prior to spreading of the free ligand molecules in chloroform solution. The solid supports used were clean quartz (1 × 5 cm) slides for UV measurements, glass slides (1 × 1 cm) for XPS, and freshly cleaved mica pieces (1 × 1 cm) for SFM. After spreading of the ligand (1.65 and 3.3 nmol/cm^2), the subphase was cooled from 20 to 5 °C to promote increase in crystallinity and 0.5−2 h later the liquid subphase was slowly drained with a motor-driven syringe.

SFM measurements were performed on a Topometrix TMX2010 Discoverer system, in intermittent contact mode, using integrated Si tip/cantilevers with resonance frequency 260−330 kHz (Nanoprobe), or in contact mode using integrated Si_3N_4 tip/cantilever with SPJ constant ~0.2 N/m (Park Scientific).

XPS measurements were performed on a commercial AXIS−HS Kratos setup, using a monochromatized Al(Ka) source (5 mA emission current at 15 KV) and pass energies of 20−80 eV. A flood gun was used for the neutralization of the surface, while the final energy scaling was determined by the support Si(2p) line (103.3 eV). Possible potential gradients across the film were estimated to be 0.1 eV at most. Spectra of reference bulk samples, for which the Si(2p) line could not be used, were scaled with respect to the Ag(3d) line. Data analysis included decomposition of the photoelectron lines into Gaussian-Lorentian components superimposed on a Shirley[19] background. The role of beam induced damage was checked by comparing the spectra of various exposure times and, finally, determining sufficiently short scans. To maintain exposure periods below 3 min for the low intensity signals (e.g., the N(1s) line) it was necessary to shift the sample between sequencing scans to fresh areas. The homogeneity of the samples on the millimeter to centimeter scale has been verified to be very good, allowing this procedure for minimizing the beam induced damage.

3. Results and Discussion

3.1. 2 × 2 Co^{2+} Grid Complex. A first indication of the interaction, at the air-aqueous solution interface, between the free ligand ***1*** and the cobalt ions in the subphase was obtained by surface pressure−area (Π-A) isotherms. Figure 1a shows very different Π-A isotherms for ligand ***1*** in chloroform solution spread onto pure water against on the surface of a 1 mM aqueous cobalt hexafluorophosphate $Co(PF_6)_2$ solution. The isotherms are consistent with formation of a water-insoluble film of the complexation product. We note that ligand ***1*** spread on a different subphase, 1 mM $Co(CH_3COO)_2$ solution, does not exhibit any increase in surface pressure, indicating formation of a water-soluble product.

To characterize the product, the films were transferred onto quartz slides and examined by UV spectroscopy. The spectrum measured from the films of ***1*** spread on pure water shows absorption bands at 230 and 280 nm (Figure 1b dashed line). The UV spectrum measured from the film of ***1*** spread on Co-$(PF_6)_2$ solution shows strong absorption bands at 280 and 357 nm (Figure 1b solid line), assigned as the ligand $\pi-\pi^*$ transitions, the latter being characteristic for 2 × 2 Co^{2+} grid complexes prepared in bulk solution.[14] For comparison, the corresponding absorption band of a single Co^{2+} complex prepared from terpyridine ligand is at 326 nm. We can conclude that a film of the 2 × 2 Co^{2+} grid complex of ***1*** has been formed in-situ at the air−solution interface.

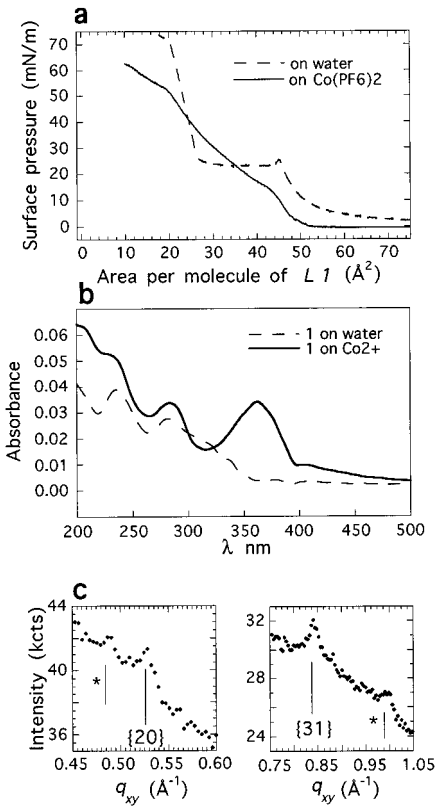

Figure 1. (a) Surface pressure−area isotherms of ligand ***1*** spread on pure water (dashed line) and on a 1 mM $Co(PF_6)_2$ aqueous solution (solid line). (b) UV spectra of the films prepared from the same amount of free ligand ***1*** spread on water (dashed line) and on a 1 mM Co-$(PF_6)_2$ aqueous solution (solid line), after transfer to quartz slides. (c) Measured GIXD pattern, $I(q_{xy})$ (for clarity, divided in two q_{xy} regions), of the film prepared by spreading ligand ***1*** on a 1 mM $Co(PF_6)_2$ aqueous solution.

Analysis of the Grazing Incidence X-ray Diffraction Data. The extent of crystallinity in the film of the 2 × 2 Co^{2+} grid complex was examined by GIXD measurements. Spreading free ligand ***1*** onto the $Co(PF_6)_2$ solution surface yielded a very weak diffraction pattern, $I(q_{xy})$, containing broad Bragg peaks (Figure 1c). On the other hand, highly crystalline films were obtained by spreading, on pure water, a very dilute ($5.4\cdot10^{-5}$ M) nitromethane solution of the corresponding preformed complex (Figure 2a). All the Bragg peaks of the GIXD pattern, $I(q_{xy})$, could be indexed with *h,k* Miller indices (Figure 2a) yielding a rectangular two-dimensional cell of dimensions $a = 23.7$ Å, $b = 21.5$ Å. The crystalline domains are anisotropic, with a coherence length, estimated from the full width at half-maximum fwhm(q_{xy}), of ~1000 Å along the *b* direction and of ~500 Å along the *a* direction. The film thickness, estimated from the fwhm(q_z) of the measured Bragg rods (shown in Figure 2b for the {10}, {20}, and {02} reflections), was found to be of 17 ± 2 Å. According to the 3-D crystal structure[14] of the $[Co_4L\mathbf{1}_4]\cdot 8SbPF_6$, the grid complex cation has a distorted $\bar{4}2m$ point symmetry. The dimensions of such a cation, ~20 × 20 × 14 Å, suggest that the crystalline film formed on water is a

(18) Jacquemain, D.; Grayer Wolf, S.; Leveiller, F.; Deutsch, M.; Kjaer, K.; Als-Nielsen, J.; Lahav, M.; Leiserowitz, L. *Angew. Chem., Int. Ed. Engl.* **1992**, *31*, 130.
(19) Shirley, D. A. *Phys. Rev. B* **1972**, *5*, 4709.

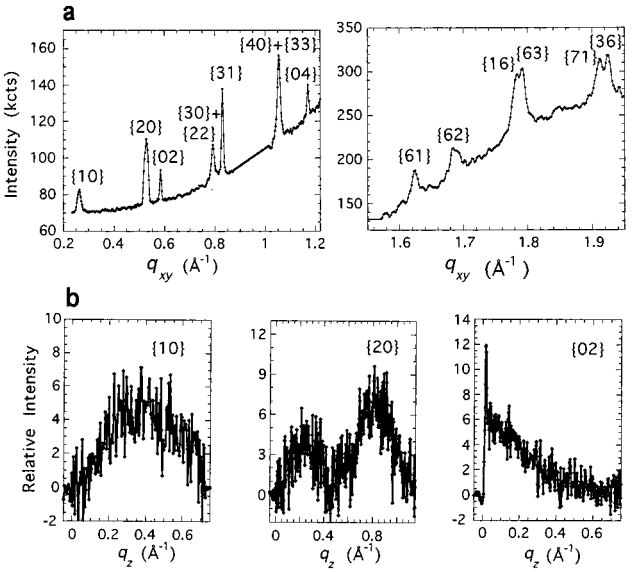

Figure 2. Measured GIXD pattern of the film prepared by spreading a nitromethane solution of the 2 × 2 Co^{2+} grid complex, as a PF_6^- salt, on water: (a) intensity distribution, $I(q_{xy})$, divided into two q_{xy} regions and (b) measured Bragg rod intensity profiles for the low-order {10}, {20}, and {02} reflections.

monolayer in which the rectangular unit cell contains a single grid complex.

The GIXD patterns obtained from the 2 × 2 Co^{2+} grid complex prepared in-situ, (Figure 1c), and the preformed complex on pure water, (Figure 2) have two reflections, {20} and {31}, at q_{xy} values of 0.53 and 0.84 Å^{-1}, in common. Apart from the poor crystallinity, the other two weak peaks of the complex prepared in-situ, which do not have a counterpart, suggest the presence of different orientations of the grids.

3.2. 3 × 3 Ag^+ Grid Complexes. We now focus on the preparation, in-situ at the air-aqueous solution interface, of films of a 3 × 3 Ag^+ grid complex, $(Ag_9L_9)\cdot 9CF_3SO_3$, starting from the two different ligands ***2*** and ***3*** (Scheme 1b,c). Unlike the 2 × 2 Co^{2+} complex, the 3 × 3 Ag^+ grid complex is unstable in dilute nitromethane solutions ($<10^{-2}$ M), and thin films are not formed by spreading more concentrated solutions on pure water. Thus the preparation of such films by reaction between the water-insoluble free ligand molecules with Ag^+ ions from the subphase represents a real challenge. A first indication of the process is given by the Π-A isotherms of the free ligands spread on water and on a 1 mM CF_3SO_3Ag solution shown in Figure 3a,b. For each system there are distinct differences in the shape of the isotherms, consistent with the formation of water-insoluble films of reaction products.[20]

In contrast to the 2 × 2 Co^{2+} grid complex, the UV spectra of the films of ligands ***2*** and ***3*** spread on water and on 1 mM CF_3SO_3Ag solution, and transferred to quartz slides, show the same absorption maxima but with stronger intensities for the latter (Figure 3c).[21] This result is compatible with the corresponding complex prepared in bulk solution.[12]

Scanning Force Microscopy Experiments. A measure of the film thickness obtained after reaction with the Ag^+ ions has been gleaned from SFM images obtained after transfer of the films from the liquid surface onto a freshly cleaved mica support. The SFM image of the film prepared from ligand ***2*** on CF_3SO_3Ag solution (Figure 4a) shows domains corresponding, essentially, to two different thicknesses. Domains of ∼5 Å height on mica were ascribed to the CF_3SO_3Ag presumably adsorbed on the mica surface before spreading of the ligand molecules.[22] Above such domains we observe slabs about 13 Å thick which we attribute to the 3 × 3 Ag^+ grid complex. Increasing the number of spread ligand molecules by a factor of 2 led to the formation of domains of ∼20 Å height (Figure 4b), in agreement with the thickness estimated from the GIXD data (see below). By comparison, the SFM images of the free ligand ***2*** show faceted crystallites ∼200−400 Å thick (Figure 4c).

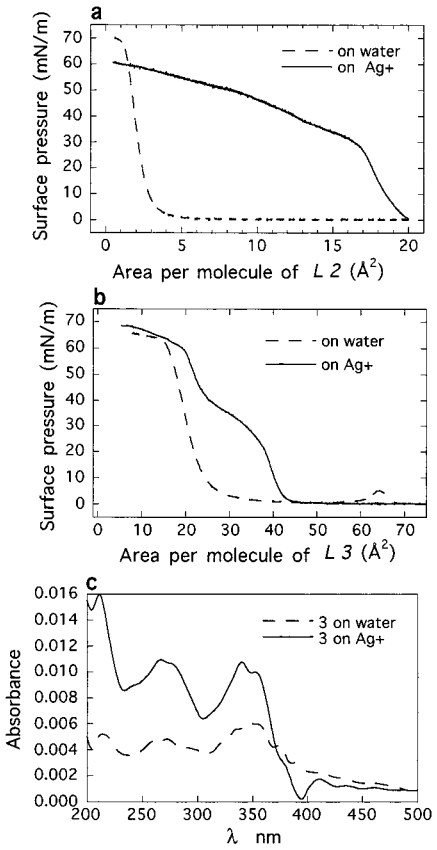

Figure 3. (a,b) Surface pressure−area isotherms of the two free ligands: (a) ***2*** and (b) ***3***, spread on pure water (dashed line) and on 1 mM CF_3SO_3Ag aqueous solution (solid line). (c) UV spectra of the films obtained from the same amount of free ligand ***3*** spread on water (dashed line) and on CF_3SO_3Ag solution (solid line), after transfer to quartz slides. Similar spectra were measured for the corresponding films of ligand ***2***.

SFM images of films prepared from the ligand ***3*** spread on water and on CF_3SO_3Ag and transferred onto mica support also show a change from faceted crystallites (Figure 4e), ∼80−150 Å thick, to thin films (Figure 4d). The thickness of the film is ∼10.5 Å, consistent with that of a monolayer as estimated by GIXD (see below).

Analysis of the X-ray Photoelectron Spectroscopy Data. An indication for the formation of the two 3 × 3 Ag^+ grid structures is provided by XPS comparing the films with two reference samples, free ligands and 3 × 3 Ag^+ grid complexes prepared in bulk solution. As shown in Figure 5a, the N(1s) line of the free ligand ***2*** consists of two components with an intensity ratio of 2:1.0 ± 0.1 and a binding energy split of 0.85

(20) Note that the isotherms of the free ligands spread on a 1 mM $AgNO_3$ solution do not show any increase in surface pressure.

(21) We were not able to make quantitative measurement of the absorption coefficients. Nevertheless, the SFM images show a homogeneous distribution of the crystallites on the solid support.

(22) Frames of 5 mm size covered only with ∼5 Å domains were also observed.

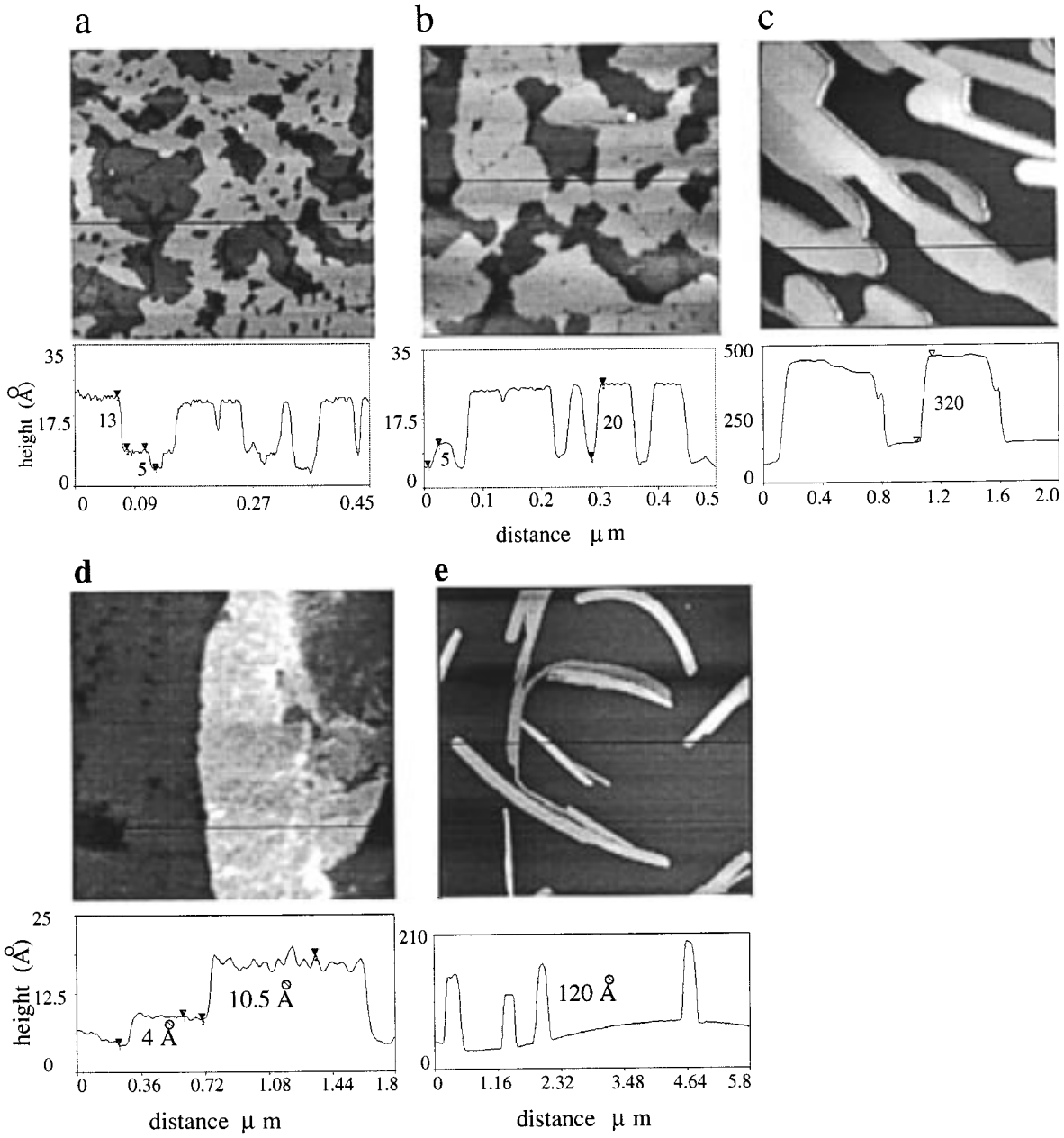

Figure 4. SFM topography images and height analyses of samples prepared by transferring, from the liquid surface onto a mica support, the films of (a,b) the 3 × 3 Ag^+ grid complex from ligand ***2***; (c) free ligand ***2*** crystallites prepared from the same amount of material as in (a) but spread on a water subphase; (d) the 3 × 3 Ag^+ grid complex from ligand ***3***; (e) free ligand ***3*** crystallites prepared from the same amount of material as in (d) but spread on water. Note that the sample in (b) contained twice the number of spread free ligand molecules than the sample in (a).

eV, attributed to the N atoms of the pyridazine ($4N_\alpha$ atoms) and pyridine ($2N_\beta$ atoms) rings, respectively. In the 3 × 3 Ag^+ grid complexes prepared in bulk solution, a pronounced shift of about 1 eV is observed for both the N(1s) (cf. Figure 5 (parts b and a)) and the C(1s) lines (cf. Figure 5 (parts e and d)). This shift reflects the coordination of the grid Ag^+ ions as well as the influence of the neighboring counterions. In fact, different N atoms are shifted by different magnitudes. A naive decomposition (not shown) of the N(1s) line (Figure 5b) into two components yields shifts of 1.5 and 1.2 eV for the N_α and N_β atoms, respectively (accompanied by pronounced broadening). However, the resultant intensity ratio, N_α:N_β = 1.5:1.0 ± 0.1, suggests that this analysis is oversimplified and that differences in binding energy, developed at the different 3 × 3 Ag^+ grid sites, should be taken into account. We can distinguish between three site types: a single central site coordinated with $4N_\alpha$ atoms, four mid-edge sites with $12N_\alpha$ and $4N_\beta$ atoms, and four vertex sites with $8N_\alpha$ and $8N_\beta$ atoms. This consideration leads to five components for the N(1s) line, three of type N_α, and two of type N_β, with fixed relative intensities. By constraining also an equal full width at half-maximum parameter, the curve-fitting procedure imposes only one additional free parameter, compared to the two-component approach, yielding an excellent fit with binding energies sequenced according to the central, mid-edge, and vertex grid sites (Figure 5b). The corresponding site-related shifts are of the order of 0.1−0.5 eV (see Table 1), with minor differences between the grids of the two ligands ***2*** and ***3***.

The film samples, prepared by spreading the free ligand molecules on aqueous CF_3SO_3Ag solution and transferred onto glass slides, exhibit spectral properties very similar to those of the bulk complexes (cf. Figure 5 (parts c,f with b,e)). We observe an identical major shift of the N(1s) and the C(1s) lines *vis-à-vis* the free ligand (cf. Figure 5 (parts c,f and a,d)), and

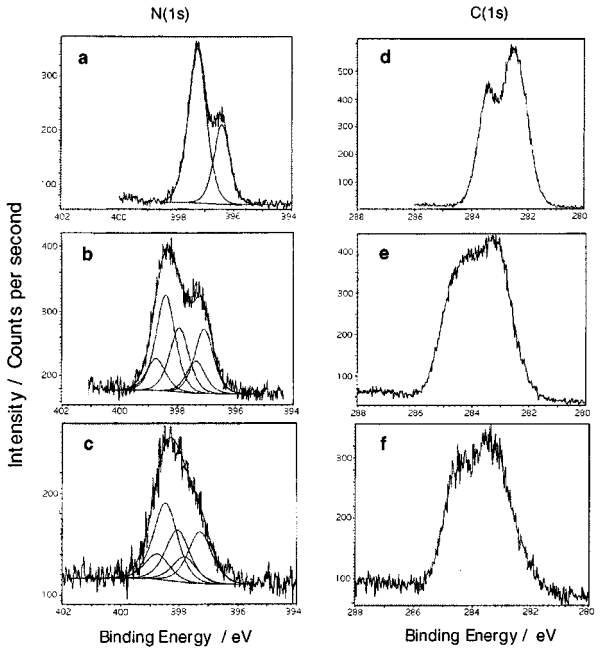

Figure 5. XPS data shown for the N(1s) line of (a) free ligand ***2***; (b) the 3 × 3 Ag^+ grid of ligand ***2*** prepared in bulk solution; and (c) a film prepared by spreading ligand ***2*** on CF_3SO_3Ag solution; (d−f) the corresponding C(1s) lines.

Table 1. Curve Fitting Results for the Site-Related Splits in the N(1s) Photoelectron Line[a]

	sample							
	bulk grid of ***2***		bulk grid of ***3***		film grid of ***2***		film grid of ***3***	
site	N_α	N_β	N_α	N_β	N_α	N_β	N_α	N_β
vertex	−0.5	−1.3	−0.35	−1.3	−0.45	−1.2	−0.55	−1.45
mid-edge	0	−1.2	0	−1.1	−0.80	−0.7	−0.80	−0.8
center	+0.15		+0.1		+0.1		+0.15	

[a] Peak positions are given in eV with respect to the mid-edge N_α atoms, which has the highest intensity. Experimental errors in peak position determination are estimated to be smaller than 0.1 eV.

closely related changes in line shape. Here too, the decomposition of the N(1s) line into two components yields an intensity ratio of approximately 1.5:1 but with considerably larger width parameters. Using the five-component approach, the site-related shifts are basically similar to the bulk complexes, except for a pronounced change in the mid-edge N_β line (Figure 5c and Table 1). We stress that the XPS spectra indicate a complete chemical reaction in the film samples; had the complexation been incomplete, a residual free ligand signal would have been observed.[23]

Thus, the XPS results suggest that the bulk and film 3 × 3 Ag^+ grid complex structures are basically similar, the differences between the two systems arising presumably from a different arrangement of the counterions.

Analysis of the Grazing Incidence X-ray Diffraction Data. The crystalline nature of the 3 × 3 Ag^+ grid films on aqueous solution was investigated by grazing incidence X-ray diffraction (GIXD). The two free ligands spread on pure water and on aqueous solution of CF_3SO_3Ag yielded crystalline domains of different structure.

(a) Ligand *2* on Water. The GIXD pattern, $I(q_{xy})$, measured for the free ligand ***2*** on water, Figure 6a, shows 12 (h,k) Bragg peaks yielding a rectangular two-dimensional (2-D) unit cell of dimensions $a = 20.01$ Å, $b = 8.12$ Å. The 2-D intensity plot $I(q_{xy},q_z)$ (Figure 6b), that displays equidistant intensity modulations along q_z, indicate the formation of multilayer crystallites in an orthorhombic unit cell with a repeat lattice spacing of 10.5 Å in the direction perpendicular to the water surface.[24] Therefore we assign Miller indices $l = 0,1,2$ to the various intensity maxima, at $q_z = 0$, 0.6, 1.2 $Å^{-1}$, of each hk Bragg rod. Powder synchrotron X-ray diffraction data from macroscopic crystalline material yielded an orthorhombic cell of dimensions $a = 20.14$ Å, $b = 8.17$ Å, $c = 10.43$ Å, space group *Pcab*. We derived a molecular packing arrangement whose calculated powder diffraction pattern[25] fitted reasonably well to that of the measured data (Figure 6c). In this arrangement the long molecular axis is parallel to the *ab* plane (Figure 6d). Since this *ab* plane of the crystalline multilayer is parallel to the water surface according to the GIXD data, we conclude that the nucleation was initiated by molecules lying flat on the water surface.[26]

(b) Ligand *2* on CF_3SO_3Ag Solution. The GIXD pattern, $I(q_{xy})$, obtained from the free ligand ***2*** spread on the surface of a CF_3SO_3Ag aqueous solution (Figure 7a), displays nine Bragg reflections. The two-dimensional intensity plot $I(q_{xy},q_z)$ shows a part of the q_{xy} range (Figure 7b). This pattern is completly different from that measured for the free ligand on pure water (Figure 6a,b) indicating that the ligand molecules, spread on the solution surface, interact with the solute ions leading to crystalline domains of a different structure.

Assuming the cell dimensions of the 3-D crystal structure of the 3 × 3 Ag^+ grid complex[12] ($a = 28.6$ Å, $b = 31.5$ Å, $c = 22.5$ Å, $\gamma = 116.4°$, space group $P112_1/n$, c unique axis for convenience) all the peaks of the 2-D powder pattern can be assigned (h,k) Miller indices (Figure 7a and Table 2). Such an assignment implies that the film on the solution surface consists of 2-D crystalline domains oriented with their *ab* planes *parallel* to the liquid surface.

The thickness of the crystalline domains, estimated from the full width at half-maximum of the measured Bragg rod intensity profiles along q_z, fwhm(q_z), (Figure 7c) is about 20 Å. This value is close to the thickness (22.5 Å) of the bilayer along the c axis in the 3-D crystal of the 3 × 3 Ag^+ grid complex (Figure 8a,b). The complex units in the 3-D crystal structure are related by centers of inversion within each *ab* layer and make interlayer contacts by 2-fold screw and by *n*-glide symmetry (Scheme 2a).[27] Unlike the 3-D crystal structure, all the measured Bragg peaks $I(h,k)$ from the film (Figure 7a) are absent for $h+k =$ odd, implying a *C*-centered cell. In other words, the unit cell of the 2-D structure (Scheme 2b) contains molecules at x,y,z and at $1/2+x,1/2+y,z$, which replace those generated by the *n*-glide symmetry at $1/2+x,1/2+y,1/2-z$, in the 3-D crystal (Scheme 2a). Thus in the 2-D crystalline domains, the

(23) XPS data of films of 2 × 2 Ag^+ grids prepared from a different ligand spread on CF_3SO_3Ag clearly show the residual free ligand; unpublished results.

(24) For some of the intensity maxima at q_z of 0.6 and 1.2 $Å^{-1}$ the intensity distribution is extended along the Scherrer lines of constant total scattering vector $q_{tot} = \mathrm{sqrt}(q_{xy}^2 + q_z^2)$. We estimate a thickness of the crystallites of 500 Å. The repeat lattice spacing is 10.5 Å ≈ $2\pi/\Delta q_z$, where Δq_z is the distance between the intensity modulations.

(25) CERIUS^2, Molecular Modeling Software for materials research from BIOSYM/Molecular Simulations Inc., San Diego, CA and Cambridge, UK.

(26) This molecular orientation is in contrast to that observed for oligothiophenes[4] on the water surface whose long molecular axis is vertical or slightly tilted from the normal to the water surface.

(27) Note that Scheme 2 depicts packing arrangements showing two layers given by empty and patterned molecules: (a) the 3-D crystal structure, where molecules *1* and *2* are related by center of inversion, *1* and *3* by 2-fold screw symmetry about an axis perpendicular to the *ab* plane, and *1* and *4* by an *n*-glide parallel to the *ab* plane; (b) the proposed bilayer structure at the air−solution interface, where molecules of type *1* and of type *3* are each related by translation, and molecules *1* and *3* by 2-fold screw symmetry.

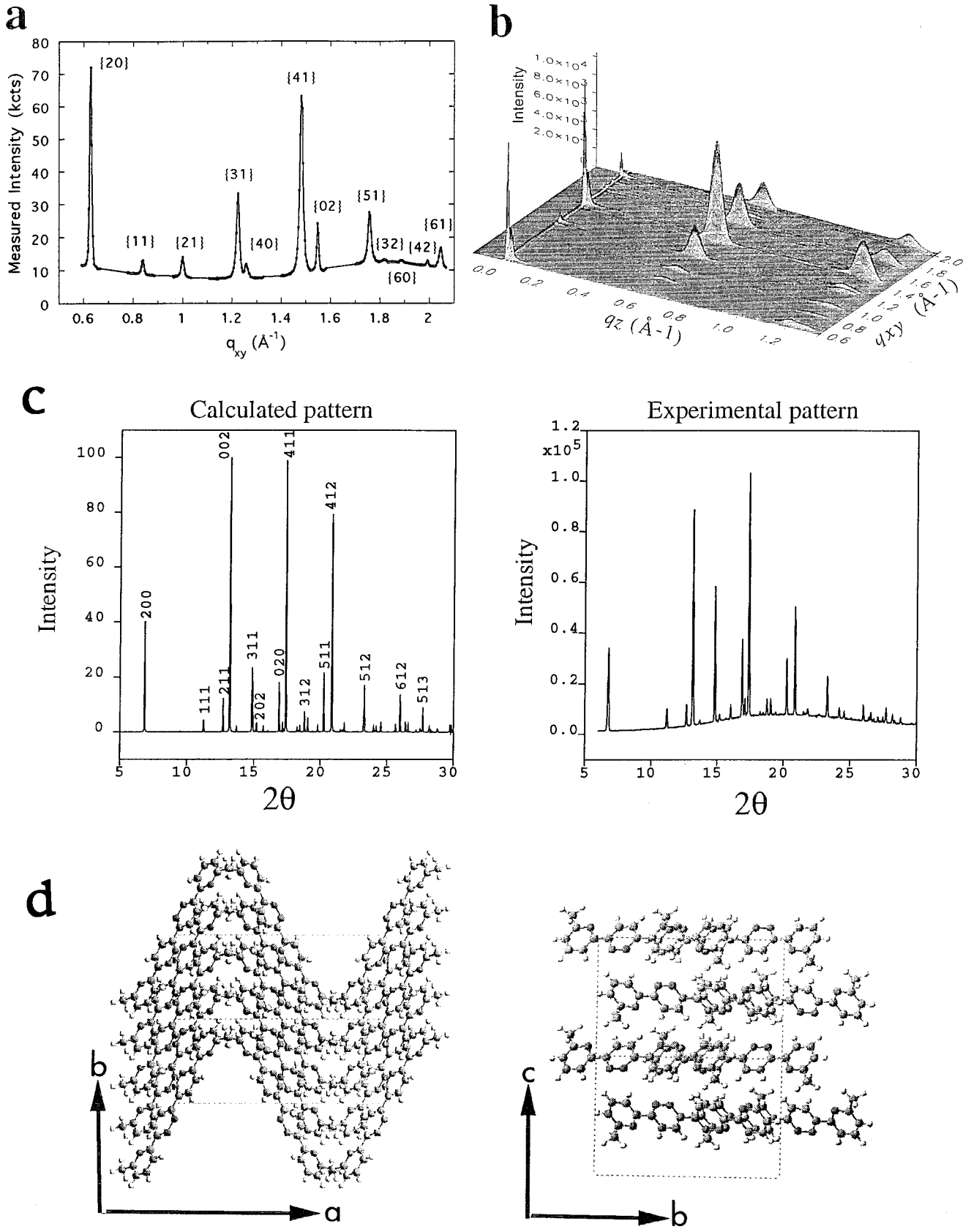

Figure 6. Measured GIXD data of ligand ***2*** spread on water: (a) intensity distribution, $I(q_{xy})$, showing the Bragg peaks; (b) two-dimensional intensity plot $I(q_{xy},q_z)$. (c) calculated (left) and measured (right) synchrotron X-ray powder pattern of the macroscopic crystalline ligand ***2*** material (wavelength $\lambda = 1.2$ Å); (d) 3-D packing arrangement of the ligand ***2*** material viewed along the *c* (left) and *a* (right) axes, corresponding to the multilayer crystallites viewed perpendicular and parallel to the water surface, respectively.

molecules within each layer are related by translation along axes $\boldsymbol{a}' = 1/2(\boldsymbol{a}+\boldsymbol{b}) = 15.9$ Å and $\boldsymbol{b}' = 1/2(-\boldsymbol{a}+\boldsymbol{b}) = 25.6$ Å, where a' and b' refer to the primitive cell derived from the *C*-centered cell (Scheme 2b and Figure 8c,d).[27] We assume that the bilayer

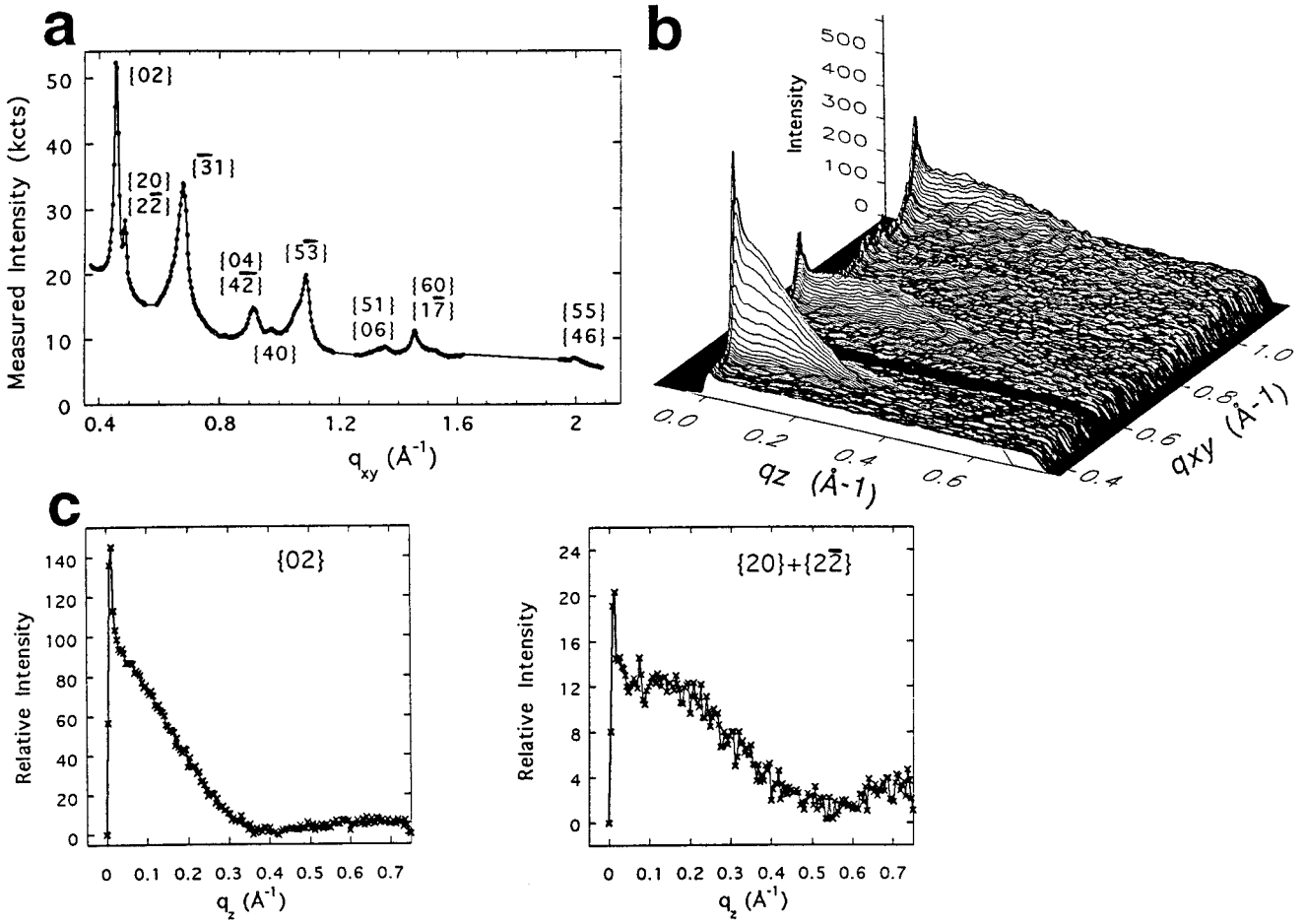

Figure 7. Measured GIXD data of ligand ***2*** spread on 1 mM $CF_3SO_3$504Ag aqueous solution: (a) intensity distribution $I(q_{xy})$ showing the Bragg peaks in the q_{xy} range 0.35−2.15 Å^{-1}; (b) two-dimensional intensity plot $I(q_{xy},q_z)$ in the q_{xy} range 0.35 to 1.15 Å^{-1}; and (c) measured Bragg rod intensity profiles for the {02} and {20}+{2$\bar{2}$} reflections.

Table 2. {*h*,*k*} Miller Index Assignment of the Measured GIXD Pattern of Ligand *2* Spread on the CF_3SO_3Ag Solution Using the 3-D Crystal Structure of the 3 × 3 Ag^+ Grid Complex

q_{xy} (Å^{-1}) obsd	{*h*,*k*} assigned	q_{xy} (Å^{-1}) calcd
0.457	{02}	0.447
0.488	{20}	0.490
	{2$\bar{2}$}	0.495
0.675	{$\bar{3}$1}	0.668
0.910	{04}	0.891
	{4$\bar{2}$}	0.879
0.980	{40}	0.981
1.085	{5$\bar{3}$}	1.082
1.350	{51}	1.341
	{06}	1.337
	{6$\bar{4}$}	1.340
	{6$\bar{2}$}	1.336
1.450	{60}	1.460
	{1$\bar{7}$}	1.466
1.990	{55}	1.989
	{46}	1.978

in the crystalline film is generated by a 2-fold screw axis perpendicular to the *ab* layer, as in the 3-D crystal, to account for the measured film thickness. In contrast to the 3-D crystal, the bilayer film does not contain a center of inversion nor an *n*-glide. We conclude that the crystalline films formed on the solution surface consists of bilayers of the 3 × 3 Ag^+ grid complex in a packing arrangement similar to but somewhat different from that of the 3-D crystal.

(c) Ligand *3* on Water and CF_3SO_3Ag Solution. Now we describe the GIXD results from thin films of a 3 × 3 Ag^+ grid from ligand ***3***, whose 3-D crystal structure is yet undetermined. We were not able to unambiguously assign a single phase to account for the GIXD pattern of the ligand ***3*** spread on pure water (Figure 9a). The GIXD pattern of ***3*** spread on CF_3SO_3-Ag solution (Figure 9b) is completely different from that on water, in agreement with crystallization of the product obtained from the interaction between the ligand and the Ag^+ ions from the subphase. We were able to assign (*h*,*k*) Miller indices to all but two very weak Bragg reflections for a single crystalline phase (Table 3). The three strongest reflections in Figure 9b have Bragg rods (Figure 9c) whose fwhm(q_z) yielded an average film thickness of 12 ± 1 Å, consistent with a monolayer film. These GIXD data indicate a single orientation of the 2-D crystallites. In addition to the pattern shown in Figure 9b, two reflections at q_{xy} values of 1.95 and 2.26 Å^{-1} (inset to Figure 9b) were observed which we assign as belonging to microcrystals of AgCl.[28]

The calculated unit cell is rectangular with dimensions a = 31.3 Å, b = 22.7 Å, γ = 90°. We may derive the number of molecules in the unit cell by comparing the "volume" per molecule here with that of the 3 × 3 Ag^+ grid complex prepared from ligand ***2***. The cell "volume" V is given by $abh\sin\gamma$, where h is the film thickness as obtained from the GIXD data. For ligand ***2*** $V_2 = 806.9 \times 20 = 16138$ Å^3, whereas for ligand ***3***, $V_3 = 710.5 \times 12 = 8526$ Å^3. V_2 contains a bilayer with four 3 × 3 Ag^+ grid complex units (volume per unit = 4036 Å^3).

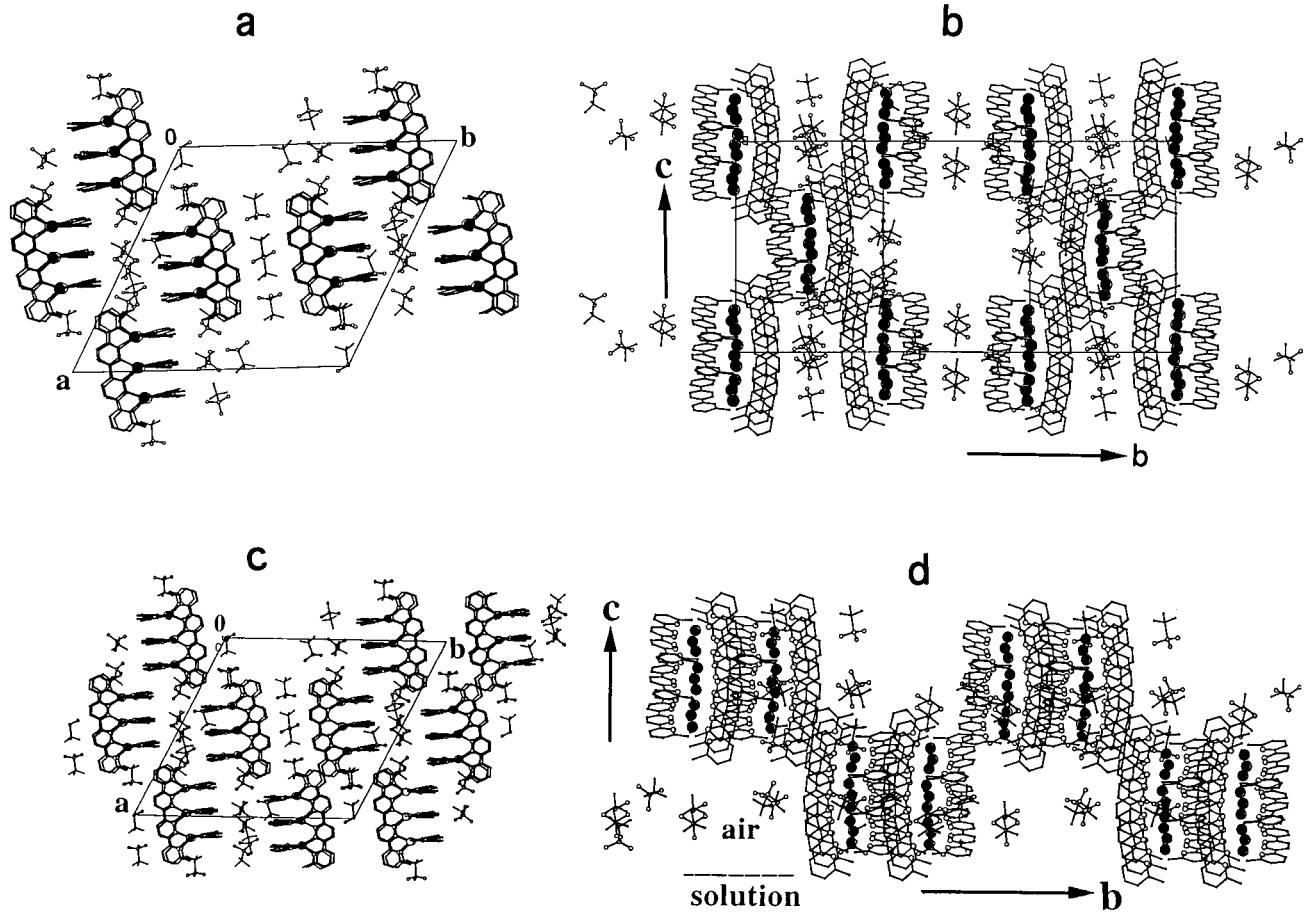

Figure 8. (a,b) Packing arrangement of the 3 × 3 Ag^+ grid complex in the 3-D crystal: (a) view perpendicular and (b) view parallel to the *ab* layer. (c,d) Proposed packing arrangement of the 3 × 3 Ag^+ grid complex units in the bilayer film prepared in-situ at the air-aqueous solution interface: (c) view perpendicular and (d) view parallel to the solution surface. Ag^+ ions are shown as filled circles.

Scheme 2

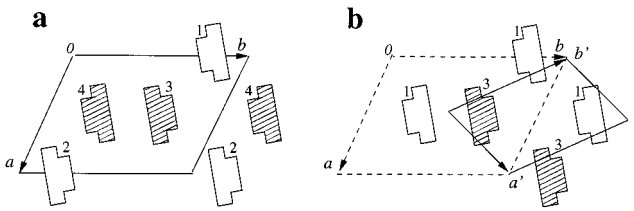

Table 3. {*hk*} Miller Index Assignment of the Measured GIXD Pattern of Ligand *3* Spread on the CF_3SO_3Ag Solution

q_{xy} (Å^{-1}) obsd	{*h*,*k*} assigned	q_{xy} (Å^{-1}) calcd
0.277	{01}	0.277
0.342	{11}	0.342
0.402	{20}	0.402
0.430		*a*
0.453		*a*
0.488	{21}	0.488
0.551	{02}	0.553
0.703	{22}	0.684
0.799	{40}	0.804
0.904	{23}	0.922
0.970	{42}	0.976

[a] These two very weak peaks are unassigned for the derived rectangular cell.

Therefore V_3 is consistent with a monolayer containing two corresponding complex units (volume per unit = 4263 Å^3). This result is also consistent with the rectangular symmetry of the unit cell containing two molecules related by either glide or a 2-fold screw symmetry, presumably along the *a* axis, since the {3,0} reflection is absent. We infer from the GIXD analysis as well as from the UV and XPS results that the monolayer film prepared from ligand ***3*** at the air−solution interface is a 3 × 3 Ag^+ grid.

Analysis of the Specular X-ray Reflectivity Data. To help ascertain the orientation of the 3 × 3 Ag^+ grid from ligand ***3***, we first compare the unit cell dimensions of this film (a = 31.3 Å, b = 22.7 Å, γ = 90°) with those of the *bc* plane in the 3-D crystal structure of the 3 × 3 Ag^+ grid from ligand ***2*** (b = 31.5 Å, c = 22.5 Å, α = 90°). From this match we deduce that the plane of the Ag^+ grid of ***3*** must lie parallel to the solution surface, in contrast to the orientation of that from ***2*** (Figure 8c,d), which is aligned perpendicular to the solution surface. These two different orientations were independently confirmed by specular X-ray reflectivity measurements performed under the same conditions as for the GIXD experiments.

The measured X-ray reflectivity curves obtained from the 3 × 3 Ag^+ grids of ***2*** and ***3*** (Figure 10) are distinctly different. The calculated curves are based on a three-box model with the constraint of the structure of the grid complexes (Scheme 1b,c) and incorporating the results from the GIXD measurements. The

(28) According to the Inorganic Powder Diffraction File, these two peaks correspond to the (111) and (200) reflections of AgCl with *d*-spacings of 3.20 Å and 2.77 Å. In contrast with all the other peaks, these two peaks are highly skewed along $q_t = (q_{xy}^2 + q_z^2)^{1/2}$ = constant. Independent GIXD measurements of other systems spread on Ag^+ containing aqueous solutions also yielded the two peaks as well as the (220) reflection with a *d*-spacings of 1.96 Å. We account for the presence of these three peaks in various systems by formation of AgCl due to the presence of traces of Cl^- ions in the compounds which were spread.

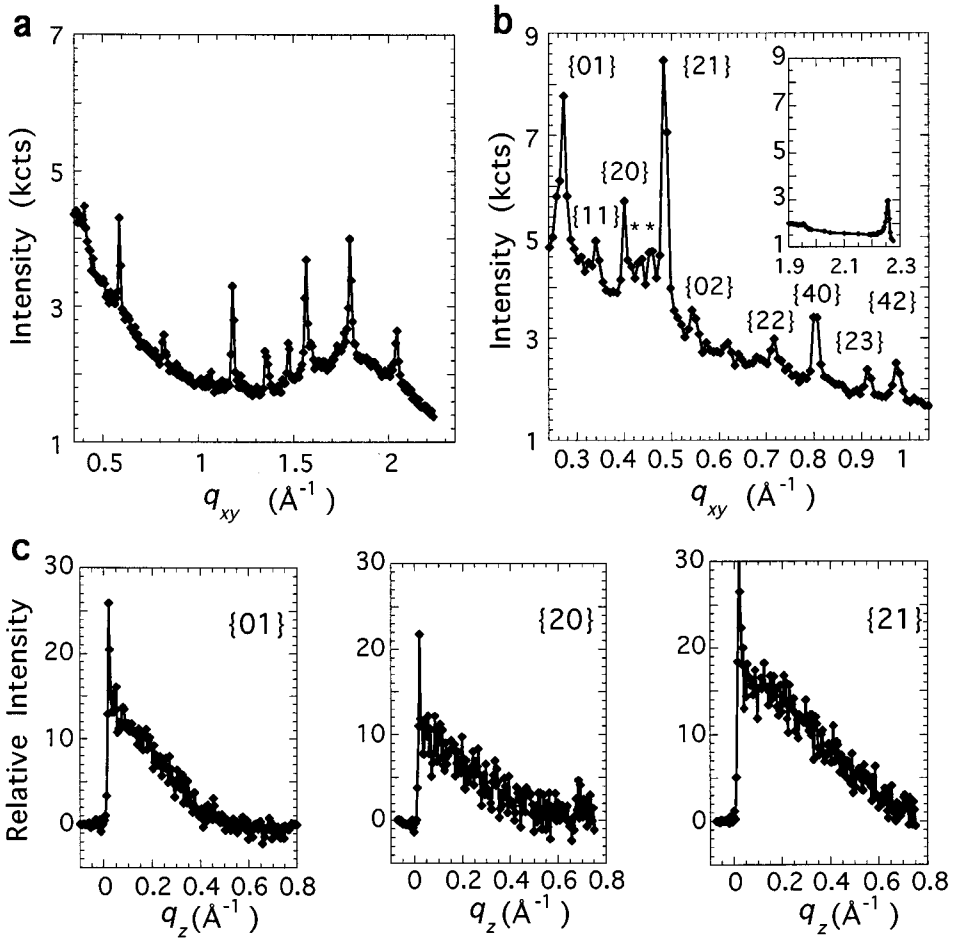

Figure 9. Measured GIXD data of ligand ***3*** spread on water and on 1 mM CF_3SO_3Ag aqueous solution. (a,b) intensity distribution $I(q_{xy})$ showing the Bragg peaks measured: (a) on water, q_{xy} range 0.35−2.25 Å^{-1}, and (b) on solution, q_{xy} range 0.24−1.04 Å^{-1}; (inset) the q_{xy} range 1.9−2.4 Å^{-1} showing the two peaks attributed to AgCl microcrystals; (c) measured Bragg rod intensity profiles for the {01}, {20}, and {21} reflections observed on solution.

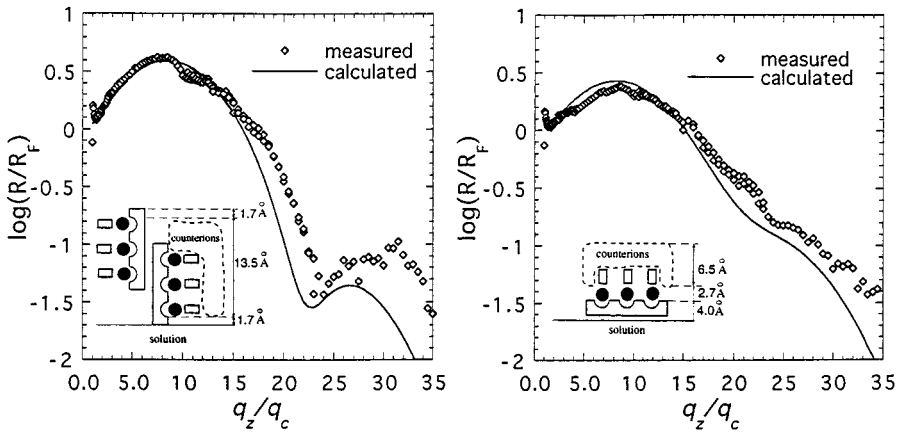

Figure 10. Measured (points) and calculated (solid line) X-ray reflectivity curves expressed as normalized R/R_F for (a) ligand ***2*** and (b) ligand ***3*** spread on 1 mM CF_3SO_3Ag aqueous solution. (Insets) schematic representation of the grid orientations in the two films.

best fits were obtained for the schematic representation of the two different orientations, shown as insets in Figure 10, and the corresponding parameters listed in Table 4. These results are in full agreement with the formation of the 3×3 Ag^+ grids from ***2*** and ***3*** as oriented crystalline films where the plane of the metal ions is either perpendicular or parallel to the solution surface.

4. Conclusions

The results described above demonstrate the formation, at the air-aqueous solution interface, of multicomponent thin film architectures, generated in-situ by interaction between water-insoluble ligand molecules and metal ions from the subphase, followed by their self-assembly into mono- or bilayer films. Three model systems were studied, two of which yielded oriented and highly crystalline films. Studies are underway for the preparation, at the air−solution and solid−solution interfaces, of other thin films of complex architectures of interest to nanotechnology. The present results add novel perspectives to self-assembly processes: they indicate first that self-assembly occurring in the bulk solution may also take place at an interface;

Table 4. Fitted Parameters[a] for the Box Model of Electron Density Corresponding to the X-ray Reflectivity Curves in Figure 10

ligand/ subphase	boxes no.	cov. %	A (Å^2)	ρ_1/ρ_s	L_1 (Å)	ρ_2/ρ_s	L_2 (Å)	ρ_3/ρ_s	L_3 (Å)	L_T (Å)	σ (Å)
2/CF_3SO_3Ag	3	65	403.5	0.38	1.7	2.07	13.5	0.38	1.7	16.9	3.6
3/CF_3SO_3Ag	3	100	354.4	1.53	4.0	1.30	2.7	1.70	6.5	13.2	3.4

[a] cov % is the surface coverage; A is the area occupied by a bilayer unit for ligand ***2*** ($0.5\ ab\sin\gamma$), and by a monolayer unit for ligand ***3*** ($0.5\ ab$); ρ_s is the electron density of the subphase, $= 0.334$e/Å^3; ρ_1 (N_1 is the number of electrons $= 87$ for ***2***, $= 726$ for ***3***), ρ_2 ($N_2 = 3772$ for ***2***, 414 for ***3***) and ρ_3 ($N_3 = 87$ for ***2***, 1310 for ***3***) are the model electron densities of the first, second, and third boxes, respectively, where $\rho_i = N_i/AL_i$, and L_1, L_2, and L_3 are the length of the boxes, respectively; the total length $L_T = L_1 + L_2 + L_3$; σ represents the surface roughness parameter.

second and more importantly, it might become possible to achieve at the gas−liquid or gas−solid interfaces the self-assembly of architectures that do not form in solution, due to interference of solvent molecules and bulk medium effects.

Acknowledgment. We thank the Israel Academy of Basic Science and Humanity, The Minerva Foundation, Münich Germany, the Danish Foundation for Natural Sciences, G. M. J. Schmidt Minerva Center for Supramolecular Architectures, and the CNRS (URA422) for financial support. We also acknowledge HASYLAB, DESY, Hamburg for beam time on beamline BW1, Prof. Bogdan Palosz and Dr. Stanislaw Gierlotka, from HPRC "UNIPRESS", Warsaw, for measuring the powder diffraction pattern of the ligand material on the beamline B2 HASYLAB, DESY, Hamburg, and Prof. P. Müller and J. Hassmann for discussions. PWB thanks the Collège de France for a research associate fellowship.

JA980205W